Thermoelectric properties of *n*-type PbTe/$Pb_{1-x}Eu_xTe$ quantum wells

A. Casian and I. Sur
Department of Informatics, Computers and Microelectronics, Technical University of Moldova, MD-2004, Chişinău, Moldova

H. Scherrer
Laboratoire de Physique des Materiaux, Ecole des Mines, Parc de Saurupt, F-54042 Nancy, France

Z. Dashevsky
Department of Materials Engineering, Ben-Gurion University of the Negev, P.O. Box 653, Beer-Sheva 84105, Israel
(Received 20 January 2000)

A systematic theoretical analysis of electronic states and thermoelectric transport in PbTe/$Pb_{1-x}Eu_xTe$ quantum well structures is presented, employing more realistic well model than has been used up to now. The carrier scattering both on optical and acoustical phonons is considered. The kinetic equations are solved using the variational method and taking into account the intersubband transitions. The electrical conductivity, thermopower (Seebeck coefficient) and thermoelectric power factor as functions of the well width are studied for quantum well (QW) structures with (100) and (111) crystallographic orientations and different carrier densities. It is found that the power factor is greater in (100) QW's, but the more realistic the well model is the lower the power factor. The dependencies of the power factor on the carrier density are determined and analyzed. It is shown that when the potential barrier height grows but the carrier density remains constant, the power factor is decreased. However the latter may be increased by increasing the permissible carrier density. So the expected values of the power factor for QW's with $U=250$ meV, $d=20$ Å, and $n=5\times10^{19}$ cm^{-3} are 175 $\mu W\,cm^{-1}\,K^{-2}$ in the case of (100) orientation and 108 $\mu W cm^{-1}\,K^{-2}$ for the (111) one. The comparison with the results of recent experiments is also presented.

I. INTRODUCTION

Interest in quantum-well structures as a new material with improved thermoelectric properties has grown considerably in the last years. This interest was stimulated by the idea[1,2] that it is possible to increase greatly the thermoelectric figure of merit ZT of certain materials by preparing them in quantum well (QW) two-dimensional (2D) layered structures. A still more significant increase in ZT was predicted for one-dimensional (1D) conductors or quantum wires.[3] These suggestions were based on the theoretical results obtained for the simplest well model; when the height of potential barriers was supposed infinite, the approximation of constant relaxation time was used and the thermal conductivity through the barriers was neglected. The main increase of ZT in these models proceeds from the large increase of the electronic density of states per unit volume that occurs when the quantum-well width decreases.

However, in systems with a finite height and a finite thickness of the potential barriers the carrier tunneling between the conducting layers leads to the formation of superlattice states and, accordingly, the density of states decreases. This effect and especially the thermal conduction through barriers tends to decrease the figure of merit[4–7] in comparison with that of idealized models. The effect of energy dependence of the relaxation time gives rise to decreasing carrier mobility with decreasing well width in 2D superlattices[8,9] and especially in 1D wires[10,11] leading to a further decrease of ZT. Thus, the significant increase of ZT, predicted in Refs. 1–3 is changed considerably. Therefore, the detailed analysis of potential thermoelectric opportunities of QW's, of expected thermoelectric efficiencies of such structures, is an important and urgent problem. Predictions about ZT in (111) and (001) oriented PbTe/PbEuTe multiple-quantum-well (MQW) structures have been presented in Ref. 12.

We have investigated[13–16] the thermoelectric opportunities of PbTe/$Pb_{1-x}Eu_xTe$ QW's in more realistic models than was done earlier. It was shown that one may obtain in (100) oriented QW's, power factor values higher than in (111) oriented structures. In Ref. 16 it was taken into account the dependence of carrier effective mass on the QW's width. This effect tends in addition to decrease ZT a little.

Experimental investigations of PbTe/$Pb_{1-x}Eu_xTe$ quantum wells[17] have shown a significant increase of the product nS^2 considered to be proportional to the thermoelectric power factor $P=\sigma S^2$, or even to ZT, where n is the carrier density, S is the Seebeck coefficient, and σ is the electrical conductivity. However, as it was demonstrated in Ref. 9, this proportionality does not hold, and with decreasing well width ZT grows much more slowly than nS^2. A real increase of the power factor was measured in the experimental work.[18] However, only (111) oriented PbTe/$Pb_{1-x}Eu_xTe$ quantum wells with $x=0.073$ were investigated. A review of the recent progress on low-dimensional thermoelectric materials for enhanced performance is presented in Ref. 19.

In the present work we investigate the thermoelectric opportunities of PbTe/$Pb_{1-x}Eu_xTe$ QW's employing the most realistic well model that was used up to now. The anisotropy of effective masses, the multivalley character of bulk semiconductors, the dependencies of effective masses on the well height and width, the presence or the lifting of valley degeneracy, the effect of carrier penetration into barriers, and the

coupling between longitudinal motion of electrons along the well and transversal motion across the well are taken into account. The electronic states in QW's are investigated as a function of the well width and of potential barrier height for structures with different crystallographic orientations. The Fermi level position and the energetic levels population are determined for different carrier concentrations. The electrical conductivity and thermopower (Seebeck coefficient) are calculated for the transport in the plane of QW by the variational method taking into consideration the intersubband transitions and the scattering of carriers both on optical and acoustical phonons. The thermoelectric power factor as a function of the well width and carrier density is determined and analyzed.

II. QUANTUM-WELL MODEL

We shall consider a quantum well formed of a thin PbTe layer of the thickness d (denoted as region 2) sandwiched between two layers of $Pb_{1-x}Eu_xTe$ (regions 1 and 3). Thus the QW structure consists of three layers, $l=1,2,3$. The electrons in the PbTe layer are confined to move into a rectangular QW potential of finite height U. The bulk PbTe and $Pb_{1-x}Eu_xTe$ with $x<0.1$ have four equivalent full valleys (energetic minima) in L points of Brillouin zone and four full ellipsoids of constant energy that are oriented in the directions [111].

In the envelope function approximation (EFA), the Hamiltonian of an electron in QW for a given valley can be written as

$$H=-\frac{\hbar^2}{2}\sum_{ij}\frac{\partial}{\partial x_i}\left(\frac{1}{m(z)}\right)_{ij}\frac{\partial}{\partial x_j}+U(z),$$

$$x_i=(x,y,z), \tag{1}$$

where x and y are in-plane axes and z is perpendicular to the QW plane. $(m^{-1})_{ij}$ is the tensor of inverse effective masses that has the same form in all three regions ($l=1,2,3$) due to identical crystal layer symmetry. In dependence of z it receives the barrier or well values, which must be calculated through longitudinal $m_{\|}$ and transversal $m_{\perp}$ bulk effective masses for different crystallographic orientations of the structure. $U(z)$ is the confinement potential of QW: $U(z)=U$, when $|z|>d/2$, and $U(z)=0$, when $|z|<d/2$, where U is the conduction-band offset between the well and barrier materials, and d is the QW width. The axis z is measured from the middle of QW.

The validity and limitations of the EFA have been investigated for different materials of QW's by comparing EFA results with the calculations performed within the tight-binding approximation[20] and pseudopotential approach.[21] It was shown that the EFA yields somewhat higher energies than the microscopic treatment, but this discrepancy is important only for very narrow wells. The very good agreement between the infrared transmission results measured experimentally in $PbTe/Pb_{1-x}E_xTe$ MQW's and EFA calculations established in Ref. 17 for wells larger than 20 Å, confirms that EFA calculations can be used to determine the positions of the subband energy levels, at least for not very narrow QW's.

Further calculations will be done for the structures with (100) and (111) orientations. Then for each of three considered regions the solution of the Schrödinger equation with the Hamiltonian (1) can be searched in the form[22]

$$\psi^l_{\mathbf{k}\alpha}(\mathbf{r})=\chi_{\mathbf{k}l}(\boldsymbol{\rho})e^{ia_lz(k_x+k_y)}\xi_{\alpha l}(z),$$

$$\mathbf{r}=(\boldsymbol{\rho},z),\quad \boldsymbol{\rho}=(x,y), \tag{2}$$

where $\chi_{\mathbf{k}l}(\boldsymbol{\rho})=S_w^{-1/2}\exp(i\mathbf{k}\boldsymbol{\rho})$ is the wave function that describes the free-electron motion along the well, S_w is the QW area, $\mathbf{k}$ is a 2D wave vector, and $\mathbf{k}=(k_x,k_y)$. The factor $\exp[ia_lz(k_x+k_y)]$ takes into account the coupling between longitudinal and transversal motion of the electron. The value of a_l depends on the valley position relative to the well plane and is determined by the values of longitudinal $m_{l\|}$ and transversal $m_{l\perp}$ effective masses of the well and of the barrier. It results from Eqs. (1) and (2) that the envelope wave functions $\xi_{\alpha l}(z)$ may be found from the equations

$$-\frac{\hbar^2}{2m_{zl}}\xi''_{\alpha l}+U(z)\xi_{\alpha l}=[E-\varepsilon_l(\mathbf{k})]\xi_{\alpha l}. \tag{3}$$

Here α denotes the number of dimensional quantization level (the bottom of respective energy subband), $\varepsilon_l(\mathbf{k})$ is the kinetic energy of the electron in the layer l, and E is the full electron energy measured from the bottom of the bulk PbTe conduction band. As a result of the difference between barrier and well effective masses ($\varepsilon_1\neq\varepsilon_2$) the envelope function depends on the wave vector $\mathbf{k}$ of electron motion along the layer.

Equations (3) can be solved exactly in each layer (well and barriers). Using the Bastard boundary condition,[23] i.e., the continuity of $m_z^{-1}d(\ln\xi)/dz$ at each layer boundary, the following equation for the energetic levels and dispersion law of electrons in the α subband may be obtained

$$pd=\alpha\pi-2\arcsin\{p/[(m_{z2}/m_{z1})^2\Delta^2-p^2]^{1/2}\}, \tag{4}$$

where

$$p^2=\frac{2m_{z2}}{\hbar^2}[E-\varepsilon_2(k)],$$

$$\Delta^2=\frac{2m_{z1}}{\hbar^2}(U+\varepsilon_1-E). \tag{5}$$

The full energy of electron is $E_\alpha(\mathbf{k})=E_\alpha+\mathcal{E}_\alpha(\mathbf{k})$, and it forms series of minisubbands. The bottom of each subband $E_\alpha=E_\alpha(0)$ is the energy of dimensional quantization, and $\mathcal{E}_\alpha(\mathbf{k})$ is the kinetic energy of the electron in αth subband.

From Eq. (4) it is seen: first, as far as the carrier masses in the barrier are greater than in the well, and thus $\varepsilon_1<\varepsilon_2$, the energy levels E_α lower in comparasion with the case when the effective masses should be the same; second, for slow carriers (small k_x,k_y) on deep well levels the dispersion law is near to $\varepsilon_2(k_x,k_y)$, i.e., it is determined by electron masses in the well, but for fast carriers it is near to $\varepsilon_1(k_x,k_y)$. The dispersion law became nonparabolic, although in the bulk materials it was considered parabolic.

It is also seen from Eqs. (3) and (4) that the formation of quasi-two-dimensional states is possible only if the condition

$E_\alpha(\boldsymbol{k}) < U + \varepsilon_1(\boldsymbol{k})$ is carried out, i.e., the full energy of electron with the wave vector $\boldsymbol{k}$ of longitudinal motion in the subband α must be less than the energy of the electron with the same $\boldsymbol{k}$ in the conduction band of the barrier. In the contrary case the well cannot capture the electrons with higher $\boldsymbol{k}$ and the discreet states α turn into the states of continuous spectrum.

Equation (4) was solved numerically. In order to compare our results with those of Ref. 17, the same approach[24] was used to calculate the band offsets for QW's and also the band gaps and band effective masses for $Pb_{1-x}Eu_xTe$. This gave $m_{||} = 0.620m_0$ (m_0 is the free-electron mass) and $m_\perp = 0.053m_0$ for PbTe, $m_{||} = 1.12m_0$ and $m_\perp = 0.076m_0$ for barrier material with $x = 0.073$ ($U = 171$ meV), and $m_{||} = 1.4m_0$ and $m_\perp = 0.094m_0$ for material with $x = 0.098$ ($U = 250$ meV). In Ref. 25 the band parameters of $Pb_{1-x}Eu_xTe$ were re-evaluated. This implies that the band gap E_g (and, accordingly, the band offset) is reduced approximately by 10 %, the longitudinal masses are reduced still smaller, whereas the transversal masses are increased by almost a factor of 1.7. However, this increase of barrier effective masses has influence on the transport only in very narrow wells. As our estimations have shown, at $d = 20$ Å the electrical conductivity decreases by about 20 %, the thermoelectric power slightly grows, and the thermoelectric power factor diminishes by about 15 %. With the increase of the well width these deflections diminish very rapidly. So as our calculations have a model character, we have used the abovementioned approach.[17] The masses m_x, m_y, and m_z at $T = 300$ K were then calculated in the well and in the barrier for (100) and (111) 2D oriented structures with $x = 0.073$ and $x = 0.098$, respectively. The results are listed in Table I of Ref. 14. In the previous papers[13–15] we have used 2D parabolic dispersion laws with these masses for the investigation of electron transport along the well layer. But this approximation is sufficiently only for thick QW's. Really, the nonparabolic dispersion law for each subband and for each d needs to be determined from Eq. (4).

In the present paper we neglect the nonparabolity, but we calculate from Eq. (4) the electron effective masses $m_x(d)$ and $m_y(d)$ at the bottom of the subband that are functions of d. Just these masses will characterize the electron transport in subbands. The estimations demonstrate that this is a rather good approximation.

Figures 1(a) and 1(b) show the dependencies of the dimensional quantization energies E_α on well width d for $U = 171$ meV. Each valley forms its set of levels (the bottom of respective subbands). In the case of (100) oriented QW, Fig. 1(a), the valley degeneracy is preserved, all four ellipsoids are equivalent, and the energy levels coincide. In the case of (111) oriented QW, the valley degeneracy is partially lifted. Therefore, it results in one set of levels arising from the longitudinal ellipsoid, which is oriented along the direction [111] or perpendicular to the QW plane (longitudinal subbands), and the other set arising from three, oblique to the [111] direction, ellipsoids (oblique subbands), Fig. 1(b).

At very small well width $d \sim 20$ Å in (100) QW, there is only one level E_1, but in (111) QW there are three, E_{1l}, E_{2l}, and E_{1ob}. With the growth of d these levels lower and at a certain value of d new levels appear. So far, as in the (111) case, the mass m_z is greater than in the (100) one, the distances between the levels in (111) QW are less, and their number is greater. Since here the dependence of effective masses on d has been taken into account, and the masses increase with decreasing d, the levels E_α are lower than in Ref. 14. Moreover, in (111) QW at $d = 20$ Å, there are not two, but three levels. All levels presented in Fig. 1 give rise to energy subbands, and all relevant electron-phonon scattering processes for both intrasubband and intersubband transitions will be considered in the study of the transport phenomena.

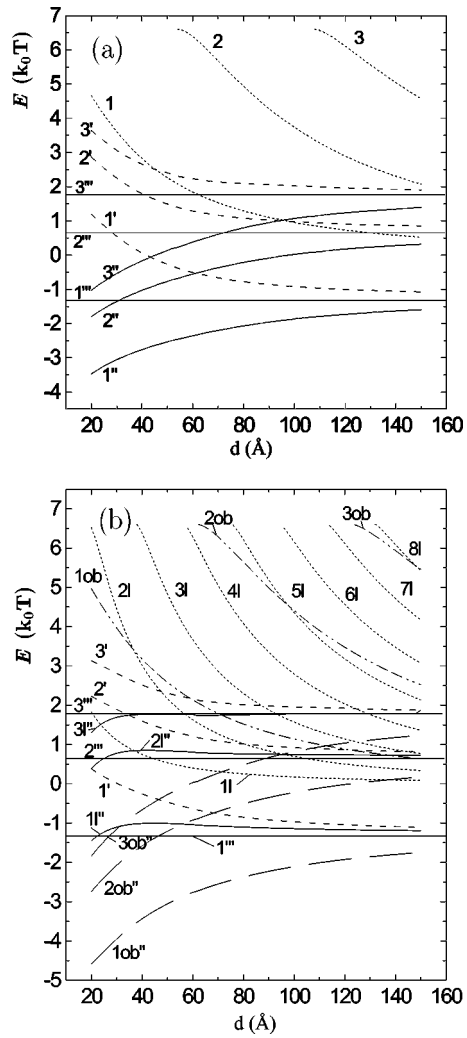

FIG. 1. (a) Quantum-well energy levels E_1, E_2, E_3 (curves 1, 2, and 3), Fermi levels E_F (curves $1'$, $2'$, and $3'$) and the differences $E_F - E_1$ (curves $1''$, $2''$, and $3''$) expressed in k_0T unites as a function of the well width d for (100) oriented $PbTe/Pb_{1-x}Eu_xTe$ wells. (b) The same as in (a) for (111) oriented wells, where the curves 1l to 8l denote the levels E_{1l}, E_{2l}, . . . , E_{8l} arising from the longitudinal ellipsoid along the [111] direction, curves 1_{ob} to 3_{ob} denote the levels E_{1ob}, E_{2ob}, and E_{3ob} arising from the oblique to [111] direction ellipsoids, curves $1l''$, $2l''$, and $3l''$ denote the differences $E_F - E_{1l}$ and curves $1''_{ob}$, $2''_{ob}$, and $3''_{ob}$ denote the differences $E_F - E_{1ob}$. Barrier height $U = 171$ meV $= 6.61k_0T(x = 0.073)$, $T = 300$ K. The levels $1'''$, $2'''$, and $3'''$ correspond to Fermi levels in bulk PbTe; $1'$, $1''$, $1'''$, $1l''$, and $1''_{ob}$ are for $n = 10^{18}$ cm^{-3}; $2'$, $2''$, $2'''$, $2l''$, and $2''_{ob}$ for $n = 5 \times 10^{18}$ cm^{-3}; $3'$, $3''$, $3'''$, $3l''$, and $3''_{ob}$ for $n = 10^{19}$ cm^{-3}.

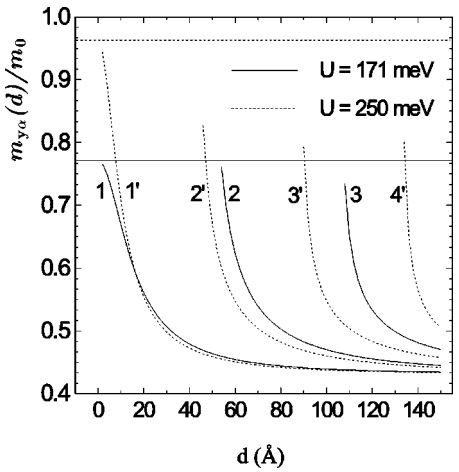

FIG. 2. Variation of electron effective masses $m_{y\alpha}(d)$ as a function of well width d in three lowest subbands of (100) QW's with $U=171$ meV (curves 1, 2, and 3) and in four subbands (curves $1'$, $2'$, $3'$, and $4'$) when $U=250$ meV. The horizontal lines note the value of effective masses in the barriers.

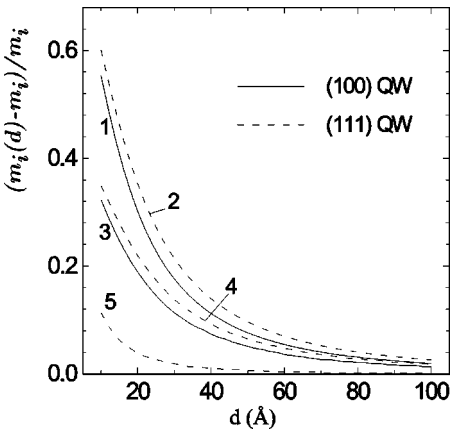

FIG. 3. Variation of relative electron effective masses as a function of the well width d in the first lowest subbands of QW's with $U=171$ meV $(i=x,y)$. Curves 1 and 3 are for m_y and m_x in the (100) well; 2 and 4 are for m_y and m_x in the lowest oblique subband of the (111) well; curve 5 is for m_y and m_x in the lowest longitudinal subband of the (111) well.

The results of the calculation of the Fermi energy E_F dependence on the well width d at fixed electron density in QW and the Fermi energies of bulk PbTe, E_F^b, for three different densities, are also shown in Fig. 1. The Fermi energy grows with the decreasing d, however, this growth is not as sharp as for E_α. Therefore, for (100) QW's the quantity E_F-E_1 that determines the degeneracy degree of 2D carriers in the respective subband, is lower than respective bulk E_F^b in the whole interval of d. There is also a large domain of parameters where $E_F-E_1<0$, and the difference $|E_F-E_1|$ increases with the decrease of d. Such behavior of E_F-E_1 is determined by increasing the density of states.

In the case of (111) QW's, the situation is more complicated because even at small d there are three levels. The difference E_F-E_{1l} is close to bulk E_F^b. Only at very small d, E_F-E_{1l} is less than E_F^b. However, for oblique subbands E_F-E_{1ob} is much lower than E_F-E_{1l} due to higher position of oblique subband than in longitudinal one.

On the base of Eq. (4) we have calculated the 2D spectrum of electrons $\mathcal{E}_\alpha(\boldsymbol{k})$ in (100) and (111) QW's for several lowest subbands. It was found that for each band the spectrum $\mathcal{E}_\alpha(\boldsymbol{k})$ is near parabolic with some new effective masses $m_{x\alpha}(d)$, $m_{y\alpha}(d)$ that depend on well width, on the subband number, and on the height of barrier potential.

Figure 2 shows, as an example, the dependence of electron effective masses $m_{y\alpha}$ on well width d in three lowest subbands of (100) QW's with $U=171$ meV and in four subbands for $U=250$ meV. It is seen that when d decreases the well masses in all subbands tend to barrier ones. At fixed d the effective mass is greater in higher subband.

Figure 3 shows the variation of relative electron effective masses $[m_i(d)-m_i]/m_i$, where $i=x,y$, in the lowest subbands for (100) and (111) QW's with $U=171$ meV. It is seen that with decreasing d the masses $m_x(d)$ and $m_y(d)$ in the longitudinal subband of (111) QW grow weakly enough because they are already close to barrier masses, but in the (100) QW and in the oblique subband of (111) QW, these masses grow considerably. This growth of effective masses is connected with the penetration of the electron wave function into the barrier. At very small d, practically the whole wave function $\xi_1(z)$ is in the barrier. With increasing d the wave function $\xi_1(z)$ becomes more and more localized in the well and the mass more and more close to well mass. The same dependence $m_{i\alpha}(d)$ is observed for the rest of the subbands.

It is interesting to note that with a precision of several percents the effective mass for any well width d may be calculated as the mathematical expectation of the well and barrier effective masses, m_i^{well} and m_i^{bar},

$$m_{i\alpha}(d)=P_\alpha m_i^{\text{well}}+(1-P_\alpha)m_i^{\text{bar}},$$

$$P_\alpha=\int_{-d/2}^{d/2}|\xi_\alpha(z)|^2dz,$$

where P_α is the quantum-mechanical probability to find the electron in the well. The increase of potential barrier height leads to the increase of effective masses as a result of barrier masses increasing.

III. THERMOELECTRIC TRANSPORT

Now we shall consider the carrier transport in the QW model, presented in Sec. II. We are interested in the transport along the QW. Therefore, let us suppose that a weak electric field $\boldsymbol{E}$ and a weak temperature gradient ∇T are applied along the well, and ∇T is parallel to $\boldsymbol{E}$. In the general case the current density $\boldsymbol{J}$ can be written in the form

$$\boldsymbol{J}=\hat{\sigma}\boldsymbol{E}-(\widehat{\sigma S})\nabla T, \tag{6}$$

where $\hat{\sigma}$ and $\hat{S}$ are the tensors of electrical conductivity and of thermopower (Seebeck coefficient), respectively. In the multivalley semiconductors the current is a sum of carrier currents from different valleys ν, so that

$$\hat{\sigma}=\sum\ \hat{\sigma}^\nu,\quad (\widehat{\sigma S})=\sum\ (\widehat{\sigma S})^\nu. \tag{7}$$

Let us further consider one valley omitting index ν. In order to determine the kinetic coefficients, it is necessary to deduce the system of kinetic equations for the nonequilibrum distribution functions $f_{\mathbf{k}\alpha}$ of electrons with the 2D wave vector $\mathbf{k}$, $\mathbf{k}=(k_x,k_y)$, in the αth 2D subband deriving from the νth valley. In Ref. 15 we have taken into account the conduction only in the lowest subband in the case of (100) QW's, or in the lowest longitudinal and oblique subbands for (111) QW's. Here more subbands and also intersubband transitions are considered, so that the problem is more complicated. To deduce the kinetic equations we used Keldysh's diagram method,[26] which is very convenient in this case. Here we shall note only the peculiarities of this deduction. In spite of the fact that the Hamiltonian (1) formally is not a sum of the Hamiltonians of longitudinal and transversal carrier motions, it is possible to obtain the kinetic equation for $f_{\mathbf{k}\alpha}$ in a well model with sharp boundaries due to the completeness and orthonormalizing properties of the function systems $\chi_{\mathbf{k}}(\boldsymbol{\rho})$ and $\exp[ia_l z(k_x+k_y)]\xi_\alpha(z)$ apart.

Further, so far as the function $\chi_{\mathbf{k}}(\boldsymbol{\rho})$ satisfies the equation,

$$\mathcal{E}_\alpha(-i\nabla_{\boldsymbol{\rho}})\chi_{\mathbf{k}}(\boldsymbol{\rho})=\mathcal{E}_\alpha(\mathbf{k})\chi_{\mathbf{k}}(\boldsymbol{\rho}),$$

it appears in the left part of the kinetic equation the velocity of the electron with the dispersion law $\mathcal{E}_\alpha(\mathbf{k})$ in the αth subband. The presence of the factor $\exp[ia_l z(k_x+k_y)]$ has influence only on the form-factor expression in the collision integral. Thus, one can obtain the kinetic equations for $f_{\mathbf{k}\alpha}$ that look like Boltzmann equations with the collision integrals of the form (the intervalley scattering is neglected)

$$I_{\mathbf{k}\alpha}=\frac{2\pi}{\hbar}\sum_{\mathbf{Q}\beta}\int d\omega A_Q^2|I_{\alpha\beta}(\mathbf{Q})|^2[N(\omega)f_{\mathbf{k}-\mathbf{q}\beta}(1-f_{\mathbf{k}\alpha}) -[N(\omega)+1]f_{\mathbf{k}\alpha}(1-f_{\mathbf{k}-\mathbf{q}\beta})]\delta[\omega-E_\alpha(\mathbf{k})+E_\beta(\mathbf{k}-\mathbf{q})] \times[\delta(\omega-\omega_{\mathbf{Q}})-\delta(\omega+\omega_{\mathbf{Q}})]. \quad (8)$$

Here A_Q is the electron-phonon matrix element. For QW's larger than 10–15 Å, the phonon confinement can be neglected and the phonons can be considered as in the bulk PbTe. Therefore for the interaction with longitudinal optical (LO) phonons, one can put

$$A_Q^2=2\pi e^2\kappa\hbar\omega_Q/(VQ^2), \quad \kappa=\varepsilon_\infty^{-1}-\varepsilon_0^{-1} \quad (9)$$

and for the interaction with deformation acoustical (DA) phonons, respectively,

$$A_Q^2=\hbar\eta Q/(2V\rho s), \quad (10)$$

where ω_Q and $N(\omega)$ are the phonon frequency and phonon distribution functions, $\mathbf{Q}$ is the 3D phonon wave vector, $\mathbf{Q}=(\mathbf{q},q_z)$, V is the volume of the system, e is the electron charge, η is the deformation potential constant, s is the sound velocity, ρ is the mass density, and ε_0 and ε_∞ are the static and high-frequency dielectric constants, respectively.

The scattering form factor in Eq. (8) is given by

$$I_{\alpha\beta}(\mathbf{Q})=\int dz\,\xi_\alpha^*(z)e^{-iz[q_z-a_l(q_x+q_y)]}\xi_\beta(z). \quad (11)$$

It is seen that in multivalley low-dimensional semiconductor structures, due to the coupling between the longitudinal and transversal motion of carriers, a supplementary item proportional to a_l, has appeared in the exponent expression from Eq. (11). For oblique subband $a_l\neq 0$, and the maximum value of the form factor $I_{\alpha\alpha}=1$ is achieved not at $q_z=0$, but at a larger value $q_z=a_l(q_x+q_y)$. The increase, characteristic for scattering values of q_z, leads to decreasing scattering probability on LO-phonons. In the case of scattering on DA-phonons this effect is small because of the quasielasticity of scattering processes.

The kinetic equations were linearized in weak field by the substitution

$$f_{\mathbf{k}\alpha}=f_{\mathbf{k}\alpha}^0-\Phi_{\mathbf{k}\alpha}\partial f_{\mathbf{k}\alpha}^0/\partial E_\alpha(\mathbf{k}), \quad (12)$$

where $f_{\mathbf{k}\alpha}^0$ is the equilibrium Fermi-Dirac distribution function, and $\Phi_{\mathbf{k}\alpha}$ is a new function, which characterizes the deflection of nonequilibrium distribution function from $f_{\mathbf{k}\alpha}^0$. The linearized equations were solved by the variational method, using for the variational function, the expression[27,28]

$$\Phi_{\mathbf{k}\alpha}=\sum_{i=1}^{2}\sum_{n=0}^{}k_i\eta_{in}\left(\frac{E_\alpha(\mathbf{k})-\zeta}{k_0T}\right)^n, \quad i=x^\nu,y^\nu, \quad (13)$$

where η_{in} are the parameters to be varied, ζ is the chemical potential, k_0 is the Boltzmann constant, T is the temperature, and x^ν and y^ν are the axes of the local coordinate system connected with the principal axes of the ellipse of constant energy $\mathcal{E}_\alpha(\mathbf{k})$ for a separate valley ν. Taking into account that the current density in the given valley is

$$\boldsymbol{J}=-\frac{2e}{V}\sum_{\mathbf{k}\alpha}\boldsymbol{v}_{\mathbf{k}\alpha}\Phi_{\mathbf{k}\alpha}\frac{\partial f_{\mathbf{k}\alpha}}{\partial E_\alpha(\mathbf{k})}, \quad (14)$$

and determining the parameters η_{in}, one can obtain the conductivity and thermopower tensors

$$\sigma_{ij}=e^2\sum_{i_1j_1nm}X_{i_1i}^n(L_{nm}^{ij})^{-1}X_{j_1j}^m, \quad (15)$$

$$(\sigma S)_{ij}=ek_0\sum_{i_1j_1nm}X_{i_1i}^n(L_{nm}^{ij})^{-1}X_{j_1j}^{m+1}, \quad (16)$$

where

$$X_{ij}^n=\frac{2}{V}\sum_{\mathbf{k}\alpha}k_i v_{k_j\alpha}\frac{\partial f_{\mathbf{k}\alpha}}{\partial E_\alpha(\mathbf{k})}\left(\frac{E_\alpha(\mathbf{k})-\zeta}{k_0T}\right)^n, \quad (17)$$

$$v_{k_j\alpha}=\frac{1}{\hbar}\frac{\partial E_\alpha(\mathbf{k})}{\partial k_j},$$

$$L_{nm}^{ij}=\frac{\pi}{\hbar k_0TV}\sum_{\mathbf{k}\mathbf{k}'q_z\alpha\beta}A_Q^2|I_{\alpha\beta}(\mathbf{Q})|^2\sinh^{-2}\left(\frac{\hbar\omega_Q}{2k_0T}\right) \times(f_{\mathbf{k}'\beta}^0-f_{\mathbf{k}\alpha}^0)\left[k_i'\left(\frac{E_\beta(\mathbf{k}')-\zeta}{k_0T}\right)^n-k_i\left(\frac{E_\alpha(\mathbf{k})-\zeta}{k_0T}\right)^n\right] \times\left[k_j'\left(\frac{E_\beta(\mathbf{k}')-\zeta}{k_0T}\right)^m-k_j\left(\frac{E_\alpha(\mathbf{k})-\zeta}{k_0T}\right)^m\right] \times\delta[\hbar\omega_Q-E_\alpha(\mathbf{k})+E_\beta(\mathbf{k}')] \quad (18)$$

and $\boldsymbol{Q}=(\boldsymbol{k}-\boldsymbol{k}',q_z)$. It is easy to see that in the coordinate system x^ν, y^ν, the matrix X_{ij}^n is the diagonal, and in the approximation of the parabolic dispersion law, used later, when $\mathcal{E}_\alpha(\boldsymbol{k})=\hbar^2k_x^2/2m_{x\alpha}+\hbar^2k_y^2/2m_{y\alpha}$, X_{ij}^n are proportional to unity matrix. The matrices of transport integrals L_{nm}^{ij} are also diagonal relative to indices i and j. As a result, the tensors σ_{ij} and $(\sigma S)_{ij}$ are reduced to principal axes.

For the calculation of the conductivity tensor, it is enough to keep in the sums on n and m, only one item with $n=m=0$. This means that in Eq. (13) only two variational parameters are used. Note that the increase of the variational parameters number leads to the corrections smaller than 5–7 %. Then, taking into account that

$$X_{ii}^0\equiv X^0=-\frac{k_0T}{\pi\hbar^2d}\sum_\alpha\sqrt{m_{x\alpha}m_{y\alpha}}F_0\left(\frac{\zeta-E_\alpha}{k_0T}\right)=-\frac{n_\nu}{\hbar}, \tag{19}$$

where $F_0(\zeta)$ is the Fermi integral of zero index and n_ν is the bulk density of electrons in νth valley, we obtain from Eqs. (15) and (18)

$$\sigma_{ii}^{-1}=-\frac{\hbar}{2e^2n_\nu^2k_0Td}\sum_{\boldsymbol{Q}\alpha\beta}q_i^2\sinh^{-2}\left(\frac{\hbar\omega_Q}{2k_0T}\right)\times A_Q^2|I_{\alpha\beta}(\boldsymbol{Q})|^2\mathrm{Im}\,\Pi_{\alpha\beta}(q,\omega_Q), \tag{20}$$

where $\mathrm{Im}\,\Pi_{\alpha\beta}(q,\omega_Q)$ is the imaginary part of the polarization operator

$$\Pi_{\alpha\beta}(q,\omega_Q)=\frac{2}{S_w}\sum_{\boldsymbol{k}}[(f_{\boldsymbol{k}\alpha}^0-f_{\boldsymbol{k}+\boldsymbol{q},\beta}^0)/(\hbar\omega+E_\alpha(\boldsymbol{k})-E_\beta(\boldsymbol{k}+\boldsymbol{q})+i\delta)],\qquad \delta\to0^+. \tag{21}$$

Here S_w is the area of QW. Let us note that if the anisotropy is neglected, expression (20) coincides with the respective expression of Ref. 29, where σ was obtained in the frame of balance equations of transport theory. If electron gas is considered pure 2D ($I_{\alpha\beta}=1$), expression (20) agrees with the results of Ref. 30), when, in the latter, the dynamical screening of the electron-phonon and electron-electron interactions is neglected.

Further simplification of Eq. (20) depends on the type of phonons. In the case of LO phonons, we have σ_{ii}^{LO}. Neglecting the phonon dispersion, $\omega_Q\equiv\omega_0$, and integrating on q_z, we obtain

$$\sum_{q_z}A_Q^2|I_{\alpha\beta}|^2=\frac{\pi e^2\kappa\hbar\omega_0}{S_wq}F_{\alpha\beta}(\boldsymbol{q}), \tag{22}$$

where form factor

$$F_{\alpha\beta}(\boldsymbol{q})=\int dz_1\int dz_2\xi_\alpha^*(z_1)\xi_\alpha(z_2)\times e^{-q|z_1-z_2|+iq_l q_y(z_1-z_2)}\xi_\beta^*(z_2)\xi_\beta(z_1)$$

also can be calculated analytically, however this expression is very cumbersome and we do not show it here.

In the case of scattering on DA phonons, the imaginary part of the polarization operator was presented in the form

$$\mathrm{Im}\,\Pi_{\alpha\beta}(q,\omega_Q)=-\frac{2\pi}{S_w}(1-e^{-\hbar\omega_Q/(k_0T)})\sum_{\boldsymbol{k}}f_{\boldsymbol{k}\alpha}^0\times(1-f_{\boldsymbol{k}+\boldsymbol{q}\beta}^0)\delta[\hbar\omega+E_\alpha(\boldsymbol{k})-E_\beta(\boldsymbol{k}+\boldsymbol{q})]. \tag{23}$$

We used the quasielasticity of scattering in the considered interval of room temperatures and carried out the expansion on $(\hbar\omega_Q/k_0T)\ll1$, assuming a linear dispersion law for DA phonon frequency ($\omega_Q=sQ$). After the integration with respect to q_z, we obtained

$$(\sigma_{ii}^{DA})^{-1}=\frac{2\pi\hbar\eta^2}{e^2n_\nu^2\rho s^2dS_w}\sum_{\boldsymbol{q}\alpha\beta}q_i^2\mathcal{I}_{\alpha\beta}\frac{1}{S_w}\sum_{\boldsymbol{k}}f_{\boldsymbol{k}\alpha}^0\times(1-f_{\boldsymbol{k}+\boldsymbol{q},\alpha}^0)\delta[E_\alpha(\boldsymbol{k})-E_\beta(\boldsymbol{k}+\boldsymbol{q})], \tag{24}$$

where the form factor

$$\mathcal{I}_{\alpha\beta}=\int dz|\xi_\alpha(z)|^2|\xi_\beta(z)|^2$$

does not depend on the wave vector $\boldsymbol{q}$ of longitudinal phonon motion.

When both scattering mechanisms on LO and DA phonons are considered, it results in one valley ν, in the local coordinate system x^ν, y^ν, $(\sigma_{ii}^\nu)^{-1}=(\sigma_{ii}^{LO})^{-1}+(\sigma_{ii}^{DA})^{-1}$. Note that the tensors σ_{ii}^ν are diagonal, but the in plane of QW 2D valley conductivities $\sigma_{x^\nu x^\nu}^\nu$ and $\sigma_{y^\nu y^\nu}^\nu$ are different. Now it is necessary to lead the tensors σ_{ii}^ν to a certain definite coordinate system x, y, connected with the QW and to sum up these conductivity tensors of all four valleys. Hence it follows that $\hat{\sigma}$ is a diagonal tensor with equal components, i.e., σ is a scalar. This is the consequence of cubic symmetry of initial materials. Thus, for (100) QW

$$\sigma_{100}=2(\sigma_{x^\nu x^\nu}^\nu+\sigma_{y^\nu y^\nu}^\nu) \tag{25}$$

and for (111) oriented QW

$$\sigma_{111}=\sigma_l+\frac{3}{2}(\sigma_{x^\nu x^\nu}^\nu+\sigma_{y^\nu y^\nu}^\nu), \tag{26}$$

where σ_l is the conductivity of longitudinal subbands.

The expressions for σ cannot be calculated analytically. The results of numerical calculation of σ are shown in Fig. 4. The values of parameters were taken from Ref. 31. The scattering both on optical and acoustical phonons was taken into account. It is found that, in the considered temperature range ($T=300$ K) the main contribution to σ comes from the scattering on optical phonons, although the scattering on acoustical phonons cannot be neglected, so the contribution of the latter is of the order of 20–30 %.

All subbands of dimensional quantization, and all intrasubband and intersubband transitions were taken into account. Note that earlier[16] we had used a more simple approximation: although for the calculation of the Fermi level all subbands were taken into consideration; for the electrical conductivity it was assumed that the electron transport oc-

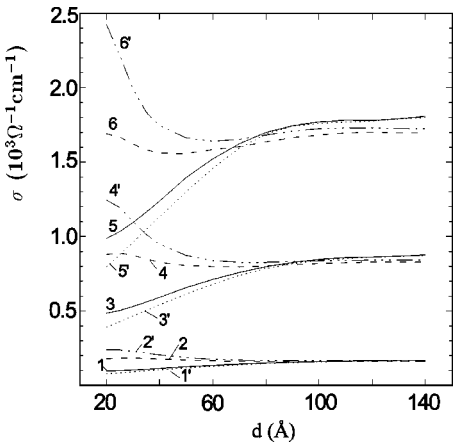

FIG. 4. Calculated electrical conductivities σ of $PbTe/Pb_{1-x}Eu_xTe$ quantum wells as a function of the well width d for (100) oriented QW's, σ_{100} (curves 1, 1′, 3, 3′, 5, and 5′) and for (111) oriented QW's, σ_{111} (curves 2, 2′, 4, 4′, 6, and 6′). Potential barrier $U=171$ meV ($x=0.073$) for the curves 1, 2, 3, 4, 5, and 6, and $U=250$ meV ($x=0.098$) for the curves 1′, 2′, 3′, 4′, 5′, and 6′, $T=300$ K. Curves 1, 1′, 2, and 2′ are for $n=10^{18}$ cm^{-3}; 3, 3′, 4, and 4′ for $n=5\times10^{18}$ cm^{-3}; 5, 5′, 6, and 6′ for $n=10^{19}$ cm^{-3}.

curs only in the one lowest subband for (100) QW or in the two lowest subbands for (111) QW. The comparison of results shows that this approximation is rather good for thin wells with $d\sim20$ Å.

As is seen from Fig. 4, when the well width d decreases, σ_{100} decreases too (curves 1, 1′, 3, 3′, 5, and 5′) although the density-of-states per unit volume increases. This behavior of σ_{100} is determined by the decrease of carrier mobility caused by the increase of the phonon wave vector region involved in the scattering processes. Namely, in the 2D case, the energy and momentum conservation laws do not impose restrictions on the projection q_z. However, due to the presence of the form factor in the collision integral, it follows that the phonons with $q_z<1/d$ are important for the scattering. Therefore, with decreasing d the scattering probability increases and σ_{100} decreases. The increase of the carrier effective mass with the decrease of d also leads to the decrease of σ_{100}. On the other hand, with decreasing d (for $d<40$ Å) the penetration of carrier wave function into barrier becomes more and more important, the wave function becomes less and less localized, the effective well width grows and the decrease of σ_{100} becomes less sharp. The increase of potential barrier height leads to the decrease of σ_{100} (curves 1′, 3′, and 5′), determined by more localized electron wave functions in deeper potential well and by the growth of effective mass, although first cause is more important. When the carrier density rises, σ_{100} grows slightly more rapidly than in the 3D case, but in all QW's σ_{100} is less than in respective bulk material.

In the (111) QW's there is another situation. As the calculation of band population shows, in very narrow QW's with $d\sim20$ Å, the main contribution to conductivity comes from the lowest longitudinal subband with small effective masses and high mobilities. Accordingly, σ_{111} is higher than σ_{100} (curves 2, 2′, 4, 4′, 6, and 6′). When d increases, the oblique subbands lower, and the electrons pass more and more from longitudinal to these subbands, due to much higher density-of-states. But in these subbands the effective masses are greater and the mobilities are smaller. Therefore σ_{111} decreases with the increasing d. The rise of the potential barrier leads to the rise of oblique subbands and, as a result, to the growth of electron population of longitudinal subbands with high mobilities. Accordingly, in spite of several increases of effective mass, σ_{111} rises. This effect is more important at small d and higher carrier density.

As is seen from Fig. 4, the highest conductivities are σ_{111} at small d, but when d grows, both σ_{100} and σ_{111} tend to the same value at a given carrier density. It is found that at $d>100$ Å the intersubband transitions and the transport in higher subbands becomes important. In this region of QW thickness the conductivity depends very slightly on the orientation of QW, on the potential barrier height, and on QW thickness d itself, tending with the growth of d to its bulk value. Note that the numerical calculations were carried out for $d>20$ Å. For smaller d the penetration of electron wave function into barrier becomes very large and it requires taking into account the scattering of carriers in barriers on alloy potential too.

IV. THERMOELECTRIC POWER

In order to determine the thermoelectric power tensor (Seebeck coefficient) S_{ij}, the tensor $(\sigma S)_{ij}$ [Eq. (16)] was calculated. The kinetic equations were also solved by variational method, using the variational function (13), but in this case, it needs to take two terms in the sum on n in Eq. (13). This means that for the calculation of S_{ij}, four variational parameters are used. Accordingly, in the sums on n and m in Eqs. (15) and (16) the terms with $n,m=0,1$ were taken into consideration.

In the matrices of transport integrals, additional components L_{01}^{ii}, L_{10}^{ii}, L_{11}^{ii} appeared, which unlike the L_{00}^{ii}, are expressed not only by the imaginary part of the polarization operator (21), but also contain more complicated structures with k_i^n under the symbol of summation in Eq. (21). The expression for S_{ij}^{ν} is rather cumbersome and cannot be presented here. Note that due to cubic symmetry of initial bulk materials the tensor $\hat{S}$ becomes a scalar, which is noted by S.

The results of the numerical calculation of S as a function of well width d for (100) and (111) oriented QW's (S_{100} and S_{111}) are shown in Fig. 5. It is seen that the highest values of S are reached in (100) QW's at small d. When d increases, the bottom of the energy subbands E_α lowers, the Fermi level E_F lowers too, but more slowly, due to the decrease of the density-of-states per unit volume. The difference $|E_F-E_\alpha|$, which influence significantly the values of S_{100}, diminish, and therefore, with increasing d, S_{100} decreases (curves 1, 1′, 3, 3′, 5, and 5′). The growth of the potential barrier from 171 meV to 250 meV has a small influence on S_{100}.

In the (111) QW's, as was mentioned above, at small d the lowest longitudinal subband is mainly populated and the most important contribution in S_{111} comes from this subband with low density-of-states. Therefore, S_{111} is less than S_{100} (curves 2, 2′, 4, 4′, 6, and 6′). When d increases, S_{111} decreases in the beginning at small d, as S_{100}. However,

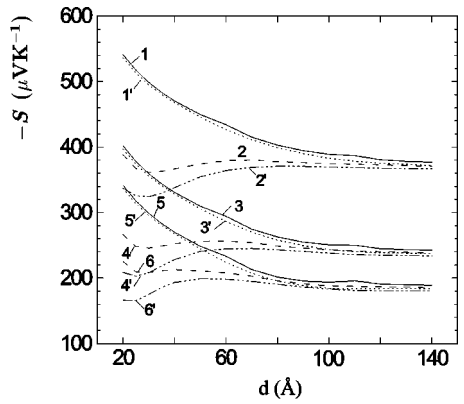

FIG. 5. Calculated thermoelectric power S of PbTe/$Pb_{1-x}Eu_xTe$ quantum wells as a function of the well width d for (100) oriented QW's, S_{100} (curves 1, 1′, 3, 3′, 5, and 5′) and for (111) oriented ones, S_{111} (curves 2, 2′, 4, 4′, 6, and 6′). Potential barrier $U=171$ meV ($x=0.073$) for the curves 1, 2, 3, 4, 5, and 6, and $U=250$ meV ($x=0.098$) for the curves 1′, 2′, 3′, 4′, 5′, and 6′, $T=300$ K. Curves 1, 1′, 2, and 2′ are for $n=10^{18}$ cm^{-3}; 3, 3′, 4, and 4′ for $n=5\times10^{18}$ cm^{-3}; 5, 5′, 6, and 6′ for $n=10^{19}$ cm^{-3}.

with futher increase of d, a weak growth of S_{111} is observed, caused by the transfer of electrons from longitudinal subbands to oblique ones, in which the density-of-states is much higher. At $d>100$ Å, the thermoelectric power depends very slightly on QW orientation, on the potential barrier height U, and on QW thickness d, tending at very large d to its bulk value.

V. THERMOELECTRIC POWER FACTOR

The above obtained values of conductivity σ and Seebeck coefficient S permit us to calculate the power factor $S^2\sigma$. Numerical results for $(S^2\sigma)_{100}$ and $(S^2\sigma)_{111}$ for (100) and (111) oriented QW's, respectively, are shown in Fig. 6 as a function of well width d. The data are presented for wells with potential barrier heights $U=171$ meV and $U=250$ meV and for several values of carrier density. It is seen that for decreasing d, the power factor increases and this growth is more pronounced at small d. In (100) QW's, due to higher values of S, the power factor $(S^2\sigma)_{100}$ is higher than $(S^2\sigma)_{111}$ in spite of lower conductivity. Nonmonotonous dependencies of $S^2\sigma$ on d arise from the peculiarities in the behavior of σ and S as functions of d, and are connected with the appearance of new subbands disposed near to the top of the potential barrier or close to the continuous energetic spectrum along the z direction. Near these values of d the criterion of calculation is broken, so in these cases the continuous spectrum needs to be taken into consideration too. The latter becomes more important at higher carrier density n when populated subband states arise near the continuous spectrum states. If in the calculation the continuous spectrum is taken into account, the nonmonotonous behavior of σ, S, and $S^2\sigma$ at high n would disappear. At the same time at large d the conductivity σ would grow slightly faster, while S and $S^2\sigma$ would decrease a little faster, when d increases, especially at higher carrier densities, tending to the respective bulk values. But for very narrow wells with $d=20$ Å, when the bottom of the first subband in (100) QW and of the first oblique (the highest) subband in (111) QW, is at least $2k_0T$ lower than the potential barrier height U, and for carrier densities such that the Fermi level E_F is at least $3k_0T$ lower than U, the contribution to the transport of the continuous spectrum may be neglected. In this case for QW with $U=171$ meV, the highest admissible carrier density is near 10^{19} cm^{-3}. At this density $(S^2\sigma)_{100}=115$ μW/cmK^2 and $(S^2\sigma)_{111}=86$ μW/cmK^2. These values practically coincide with those, which were calculated in Ref. 16 in the approximation, when only the lowest subbands were taken into account, confirming that this approximation can be applied. These values of $S^2\sigma$ are considerably higher than the measured[18] value of 38 μW/cmK^2 in the best bulk PbTe at optimal density $n=6\times10^{18}$ cm^3, and are also higher than the calculated value for large wells $d\sim150$ Å, and $n=10^{19}$ cm^{-3}, which is a little less than 60 μW/cmK^2. The enhancement of the thermoelectric power factor obviously demonstrates the effect of quantum confinement.

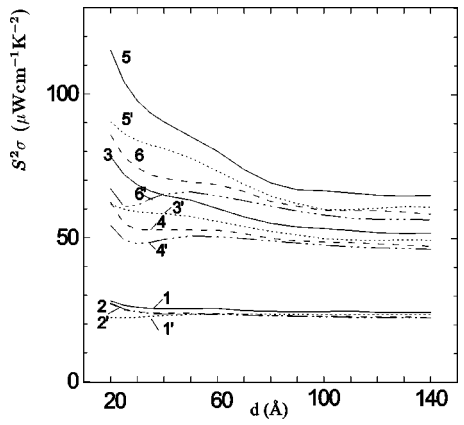

FIG. 6. Thermoelectric power factor $S^2\sigma$ of PbTe/$Pb_{1-x}Eu_xTe$ quantum wells as a function of the well width d for (100) oriented QW's, $(S^2\sigma)_{100}$, (curves 1, 1′, 3, 3′, 5, and 5′) and for (111) oriented ones, $(S^2\sigma)_{111}$ (curves 2, 2′, 4, 4′, 6, and 6′). Potential barrier $U=171$ meV ($x=0.073$) for the curves 1, 2, 3, 4, 5, and 6, and $U=250$ meV ($x=0.098$) for the curves 1′, 2′, 3′, 4′, 5′, and 6′, $T=300$ K. Curves 1, 1′, 2, and 2′ are for $n=10^{18}$ cm^{-3}; 3, 3′, 4, and 4′ for $n=5\times10^{18}$ cm^{-3}; 5, 5′, 6, and 6′ for $n=10^{19}$ cm^{-3}.

It is of interest to compare calculated values of σ, S, and $S^2\sigma$ with those that were measured[18] in PbTe/$Pb_{1-x}Eu_xTe$ (111) QW's with $x=0.073$ ($U=171$ meV) at 300 K. We shall not discuss the sample No. T-225 with very high conductivity, which is 25% greater than the calculated one. Another eight samples may be divided into two groups: four samples with narrow, $d\sim20$ Å QW's and four samples with ''large,'' $d\sim40$ Å, QW's. For the first group, the calculated conductivities σ^{cal} are greater than the experimental ones σ^{ex} on average by 50%. It is natural because not all scattering mechanisms were taken into consideration. As a result of the overestimation of σ^{cal}, S^{cal} are smaller than S^{ex} on average by 4%, but this deflection is in the limits of measurement error. Calculated power factors are greater than experimental ones on average by 25%. Thus, the theoretical data agree very well with experimental ones. For other group, σ^{cal} are greater than σ^{ex} on average by 20%, S^{cal} are greater than S^{ex} on average by 50%, and $(S^2\sigma)^{cal}$ are greater

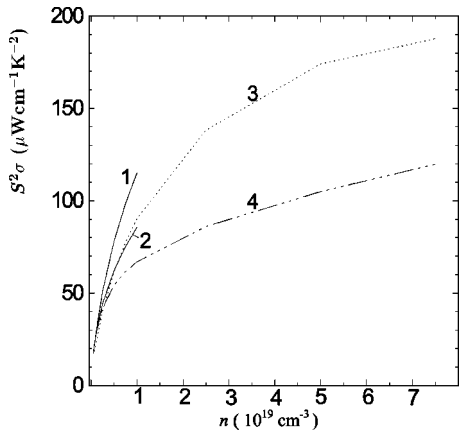

FIG. 7. Thermoelectric power factor $S^2\sigma$ of PbTe/$Pb_{1-x}Eu_x$Te quantum wells as a function of carriers concentration n for (100) oriented QW's (curves 1 and 3) and for (111) oriented ones (curves 2 and 4); $d=20$ Å, $T=300$ K. Curves 1 and 2 are for $U=171$ meV ($x=0.073$); curves 3 and 4 are for $U=250$ meV ($x=0.098$).

than $(S^2\sigma)^{ex}$ on average by 170%. The data agrees less, apparently, because near $d=50$ Å a new subband close to the height of the potential barrier appears, and the calculations are less precise for this d (the continuous spectrum was not taken into account).

When the potential barrier height grows from $U=171$ meV to $U=250$ meV, and n remains fixed, the power factor diminishes, as is seen in Fig. 6. This effect is determined by the diminution of σ and S, caused by more localized wave functions in a deeper potential well. But in deeper wells the possibility of raising the optimal carrier density appears. Figure 7 shows the results of the power factor $S^2\sigma$ calculation as a function of carriers density for (100) and (111) oriented QW's with $U=171$ meV and $U=250$ meV, respectively. The well thickness is taken equal to 20 Å for which the greatest increase of $S^2\sigma$ is achieved. For $n\leqslant 10^{19}$ cm^{-3} the growth of $S^2\sigma$ is especially sharp. With the further increase of n when the effect of carrier degeneration begins to manifest itself, the growth of $S^2\sigma$ is reduced, but it lasts up to $n\sim 10^{20}$ cm^{-3}. For higher densities n, when $U=250$ meV, or for $n>10^{19}$ cm^{-3}, when $U=171$ meV, the theory is not applicable, since the carrier continuous spectrum becomes important, and it was not taken into consideration. As Fig. 7 shows, the expected values of the power factor for $U=250$ meV, $d=20$ Å, and $n=5\times 10^{19}$ cm^{-3} are $(S^2\sigma)_{100}=175$ μW/cmK^2 and $(S^2\sigma)_{111}=108$ μW/cmK^2, which are, respectively, 4.6 and 2.8 times higher than the above-mentioned best bulk PbTe value, or 3.1 and 1.9 times higher than the calculated value for large wells with $d\sim 150$ Å, $U=171$ meV, and $n=10^{19}$ cm^{-3}, or 1.5 and 1.3 times higher than respective values for $d=20$ Å and $U=171$ meV. These results look very promising.

Unfortunately, we can not evaluate here the thermoelectric figure of merit $ZT=S^2\sigma T/\kappa$, because the thermal conductivity κ of the structure with QW or even that of the QW itself was not calculated. This problem is rather complicated and, to our knowledge, it is not yet solved. Theoretical investigations[32–34] have shown a decrease of thermal conductivity of superlattices. A reduction of the in-plane thermal conductivity in superlattices has also been observed experimentally.[35,36] Thus we can expect that the thermal conductivity of thin QW's will be smaller than that of bulk material.

Finally we note that if one takes the value of $Z_{2D}T=0.78$ or maybe 1.23 obtained in Ref. 18 for PbTe/$Pb_{1-x}Eu_x$Te (111) QW's with $U=171$ meV, $d=20$ Å, $n=1.1\times 10^{19}$ cm^{-3}, we expect to obtain for (100) QW's $Z_{2D}T$ values of the order of 1.1 or even 1.7, or slightly greater for QW's with higher potential barrier and higher electron concentrations, but not so high as was predicted in the first publications.[1,2]

VI. CONCLUSIONS

Thermoelectric properties of *n*-type multivalley PbTe/$Pb_{1-x}Eu_x$Te quantum wells are investigated theoretically. The results for electrical conductivity σ, thermoelectric power S, and thermoelectric power factor $S^2\sigma$ reported in this paper, extend previous investigations to a more realistic well model, higher carrier concentrations, and larger wells. It is shown that with decreasing well width d, the effective masses in the well increase and tend to barrier masses. The 2D carriers energetic spectrum and thermoelectric transport is calculated taking into account this effect. Intrasubband and intersubband scattering both on acoustical and optical phonons is considered. The kinetic equations are solved by variational method and analytical expressions for electrical conductivity and Seebeck coefficient are obtained. Numeric calculations are made for structures with (100) and (111) crystallographic orientations and different carrier concentrations.

It is shown that for (100) structures, σ_{100} decreases with decreasing well width d, but S_{100} and $(S^2\sigma)_{100}$ increase. In the case of (111) orientation, σ_{111} grows with decreasing d, S_{111} at first slightly decreases and then increases for the smallest width, and $(S^2\sigma)_{111}$ grows. The power factor is greater in (100) oriented quantum wells than in (111) ones in the whole interval of variation of d. Calculated values of electrical conductivity, thermopower, and the power factor are in good qualitative agreement with the data[18] measured in (111) multiple-quantum-well structures with $x=0.073$ ($U=171$ meV), $d\sim 20-23$ Å and $n\sim 6\times 10^{18}-1.1\times 10^{19}$ cm^{-3}. At very large d the values of σ, S and $S^2\sigma$ do not depend on well orientation and tend to values for bulk PbTe at given carrier concentration n.

The increase of the potential barrier height U give rise to the decrease of the power factor, mainly because of the more localized carrier wave functions in a deeper quantum well. It is shown, that in this case, the possibility appears to increase the permissible carrier concentration. Thus for $U=250$ meV the concentration may be raised up to nearly 10^{20} cm^{-3}. The expected values of the power factor for $n=5\times 10^{19}$ cm^{-3} and $d=20$ Å become $(S^2\sigma)_{100}=175$ μW/cmK^2 and $(S^2\sigma)_{(111)}=104$ μW/cmK^2, respectively, for (100) and (111) QW's. Possible values of the figure of merit are also discussed, and it is predicted that they could achieve $1.1-1.7$ in (100) oriented QW's. Unfortunately, more precise predictions about the values of the fig-

ure of merit cannot be presented now because the thermal conductivity of $PbTe/Pb_{1-x}Eu_xTe$ QW's have not been calculated yet. This problem is of special importance in order to determine the optimal thermoelectric properties of such structures.

ACKNOWLEDGMENTS

The authors would like to thank V. Kantser and A. Sandu for useful discussions. This work was supported by INTAS under the Contract No. 96-0535.

[1] L. D. Hicks and M. S. Dresselhaus, Phys. Rev. B **47**, 12 727 (1993).
[2] L. D. Hicks, T. C. Harman, and M. S. Dresselhaus, Appl. Phys. Lett. **65**, 3230 (1993).
[3] L. D. Hicks and M. S. Dresselhaus, Phys. Rev. B **47**, 16 631 (1993).
[4] J. O. Sofo and G. D. Mahan, Appl. Phys. Lett. **65**, 2690 (1994).
[5] P. J. Lin-Chung and T. L. Reinecke, Phys. Rev. B **51**, 13 244 (1995).
[6] D. A. Broido and T. L. Reinecke, Phys. Rev. B **51**, 13 797 (1995).
[7] D. A. Broido and T. L. Reinecke, Appl. Phys. Lett. **67**, 1170 (1995).
[8] A. Knipp and T. L. Reinecke, Phys. Rev. B **48**, 5700 (1993).
[9] T. L. Reinecke and D. A. Broido, Mater. Res. Soc. Symp. Proc. **478**, 161 (1997).
[10] H. Scherrer, S. Scherrer, A. Casian, I. Sur, and A. Sandu, Phys. Low-Dimens. Semicond. Struct. **10**, 77 (1997).
[11] A. Casian, J. Sur, A. Sandu, H. Scherrer, and S. Scherrer, in *Proceedings of the 16th International Conference on Thermoelectrics: Proceedings ICT'97*, Dresden, Germany, edited by A. Heinrich and J. Schuman (IEEE, Piscataway, NJ, 1997), p. 26.
[12] T. Koga, S. B. Cronin, T. C. Harman, and M. S. Dresselhaus, Mater. Res. Soc. Symp. Proc. **490**, 263 (1998).
[13] A. Casian, Z. Dashevsky, V. Kantser, H. Scherrer, I. Sur, and A. Sandu, in *Proceedings of the 17th International Conference on Thermoelectrics: ICT'98*, Norgoya, Japan, edited by Kunihito Kuamoto (IEEE, Piscataway, NJ, 1998), p. 51.
[14] A. Casian, Z. Dashevsky, H. Scherrer, S. Scherrer, I. Sur, and A. Sandu, J. Thermoel. **3**, 29 (1998).
[15] A. Casian, Z. Dashevsky, H. Scherrer, S. Scherrer, I. Sur, and A. Sandu, J. Thermoel. **1**, 59 (1999).
[16] H. Scherrer, Z. Dashevsky, V. Kantser, A. Casian, I. Sur, and A. Sandu, Mater. Res. Soc. Symp. Proc. **545**, 99 (1999).
[17] L. D. Hicks, T. C. Harman, X. Sun, and M. S. Dresselhaus, Phys. Rev. B **53**, 10 493 (1996).
[18] T. C. Harman, D. L. Spears, and M. J. Manfra, J. Electron. Mater. **25**, 1121 (1996).
[19] M. S. Dresselhaus, G. Dresselhaus, X. Sun, Z. Zhang, S. B. Cromn, and T. Koga, Solid State Phys. **41**, 755 (1999).
[20] T. G. Dargam, R. B. Capaz, and Belita Koiler, Phys. Rev. B **56**, 9625 (1997).
[21] F. Long, W. E. Hagston, and P. Harrison, in *Proceedings of the 23rd International Conference on the Physics of Semiconductors*, edited by M. Shefler and R. Zimmermann (World Scientific, Singapore, 1996), p. 819.
[22] T. Ando, A. B. Fowler, and F. Stern, Rev. Mod. Phys. **54**, 437 (1982).
[23] G. Bastard, J. A. Brum, and R. Ferreira, Solid State Phys., Adv. Res. Appl. **44**, 229 (1991).
[24] Shu Yuan, G. Springholz, G. Bauer, and M. Kriechbaum, Phys. Rev. B **49**, 5476 (1994).
[25] Shu Yuan, H. Krenn, G. Springholz, Y. Veta, G. Bauer, and P. G. McCann, Phys. Rev. B **55**, 4607 (1997).
[26] L. V. Keldysh, Zh. Éksp. Teor. Fiz. **47**, 1515 (1964) [Sov. Phys. JETP **20**, 1018 (1964)].
[27] J. Ziman, *Electrons and Phonons* (Clarendon Press, Oxford, 1960), Chap. 10.
[28] P. N. Gorlei and V. A. Shenderovsky, *Variational Method in Kinetic Theory* (Naucova Dumka, Kiev, 1992), Chap. 3 (in Russian).
[29] X. L. Lei, J. L. Birman, and C. S. Ting, J. Appl. Phys. **58**, 2270 (1985).
[30] A. I. Kasiyan (A. Casian), I. V. Sur, and I. I. Balmush, Fiz. Tekh. Poluprovodn. **25**, 689 (1991) [Sov. Phys. Semicond. **25**, 415 (1991)].
[31] Yu. I. Ravich, B. A. Efimova, and I. A. Smirnov, *Methods of Investigation of Semiconductors Applied to Lead Chalcogenides PbTe, PbSe, PbS* (Nauca Press, Moscow, 1968), Annex B.
[32] Per Hyldgoard and G. D. Mahan, Phys. Rev. B **56**, 10 754 (1997).
[33] G. Chen, J. Heat Transfer **119**, 220 (1997).
[34] L. I. Anatychuk, S. V. Melnichuk, and A. V. Kosyachenco, J. Thermoel. **3**, 61 (1998).
[35] X. Y. Yu, G. Chen, A. Verma, and J. S. Smith, Appl. Phys. Lett. **67**, 3554 (1995).
[36] S.-M. Lee, D. Cahill, and R. Vencatasubramanian, Appl. Phys. Lett. **70**, 2957 (1997).